

Noiseless photonic non-reciprocity via optically-induced magnetization

Xin-Xin Hu,^{1,3,*} Zhu-Bo Wang,^{1,3,*} Pengfei Zhang,^{2,4,†} Guang-Jie Chen,^{1,3} Yan-Lei Zhang,^{1,3} Gang Li,^{2,4} Xu-Bo Zou,^{1,3} Tiancai Zhang,^{2,4} Hong X. Tang,⁵ Chun-Hua Dong,^{1,3,‡} Guang-Can Guo,^{1,3} and Chang-Ling Zou^{1,3,2,§}

¹CAS Key Laboratory of Quantum Information, University of Science and Technology of China, Hefei 230026, P. R. China.

²State Key Laboratory of Quantum Optics and Quantum Optics Devices,
and Institute of Opto-Electronics, Shanxi University, Taiyuan 030006, China

³CAS Center For Excellence in Quantum Information and Quantum Physics,
University of Science and Technology of China, Hefei, Anhui 230026, P. R. China.

⁴Collaborative Innovation Center of Extreme Optics, Shanxi University, Taiyuan 030006, China

⁵Department of Electric Engineering, Yale University, New Haven, CT 06511, USA

(Dated: August 16, 2021)

The realization of optical non-reciprocity is crucial for many device applications, and also of fundamental importance for manipulating and protecting the photons with desired time-reversal symmetry. Recently, various new mechanisms of magnetic-free non-reciprocity have been proposed and implemented, avoiding the limitation of the strong magnetic field imposed by the Faraday effect. However, due to the difficulties in suppressing the drive and its induced noises, these devices exhibit limited isolation performances and leave the quantum noise properties rarely studied. Here, we demonstrate a new approach of magnetic-free non-reciprocity by optically-induced magnetization in an atom ensemble. Excellent isolation of signal (highest isolation ratio is $51.4^{+6.5}_{-2.5}$ dB) is observed over a power dynamic range of 7 orders of magnitude, with the noiseless property verified by quantum statistics measurement. The approach is applicable to other atoms and atom-like emitters in solids, paving the way for future studies of integrated photonic non-reciprocal devices, unidirectional quantum storage and state transfer, as well as topological photonics technologies.

I. INTRODUCTION

Lorentz reciprocity and its violation, associating with the time-reversal symmetry breaking, are of fundamental and conceptual importance in optics [1–3], and have also led to controversies in the photonics research community [4]. In practical optical applications, non-reciprocal optical devices, including isolator, circulator, and gyrator, are indispensable and ubiquitous. The prominent mechanisms realizing the optical non-reciprocity are the magnetic circular dichroism and circular birefringence (Faraday effect) in bulky magneto-optical materials [5, 6]. A strong magnetic bias field changes the dipole momentum or transition frequencies of dielectrics by inducing the Zeeman splitting of electron spin states and modifying the electronic wavefunctions, thus breaks the reciprocity of light [3]. However, limited by magnetic shields, material processing, switching response and re-configurability, the utilization of conventional non-reciprocal devices is restricted in many scenarios, such as photonic integrated circuits [7, 8] and hybrid superconducting-photonic systems [9, 10].

Over the past decade, great efforts have been dedicated to realizing magnetic-free non-reciprocity of light [3]. Ingenious ideas and new experimental techniques are developed to break the limit of the conventional Faraday effect, such as optical drive induced directional frequency conversion [11–14], storage [15–17] or amplification [18–21], the synthetic magnetic field in a loop of coupled-resonator [22, 23], and RF/acoustic drive induced spatio-temporal modulation of refraction index [24–27]. The common principle behind these approaches is the orbital momentum conservation in the coherent mode conversions, which induces absorption or phase shift for pho-

tons input from a selected direction. However, such mechanism imposes limitations for non-reciprocal devices, such as the stringent phase-matching condition, drive-induced noises via the intermediate excitations or nonlinear wave-mixing processes, giving rise to non-ideal performances. For example, the quantum properties of the isolators are not tested experimentally, and the achievable isolation ratio is less than 20 dB [8, 11–13, 16–19].

Here, we propose and demonstrate a new scheme to realize the non-reciprocity via the optically-induced magnetization (OIM) of an atomic medium. Isolation ratios of $30.3^{+0.3}_{-0.2}$ dB and $51.5^{+6.5}_{-2.5}$ dB are realized with a warm atom vapor in free space and in a traveling-wave cavity, respectively. Dispersive non-reciprocal effects analogous to Faraday effect are also observed with a non-reciprocal optical mode frequency splitting exceeding 100 MHz. It is worth noting that the non-reciprocal photon-atom interaction was investigated previously [28, 29], however, under the requirement of tens of Gauss bias magnetic field. The magnetic-free OIM mechanism is distinct by treating the atom ensemble as a magnetizable dielectric medium, where incoherent population transfer could be utilized for achieving the non-reciprocity. Its crucial advantages include that the optical drive frequency could be far detuned from the signal, avoiding the difficulty associated with phase matching and drive filtration, robustness against drive fluctuations, and elimination of drive-induced noises at signal frequencies. We show that the equivalent intracavity noise excitation introduced by the device is less than 10^{-2} , proving the inherent noiseless property of this mechanism. We believe that our experiments could stimulate further experimental and theoretical efforts on OIM, to demonstrate non-reciprocal devices in photonic integrated circuits, and find applications in

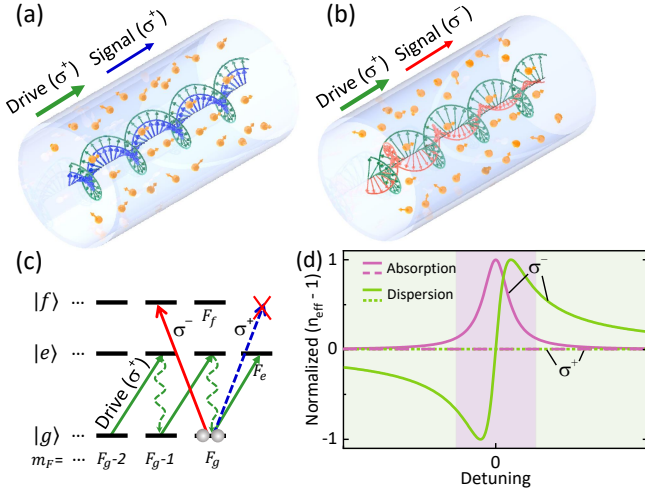


FIG. 1. **Schematic of circular birefringence and circular dichroism arising from optically-induced magnetization.** (a) and (b) In an atomic medium with non-zero magnetization induced by a σ^+ -polarized drive field, the σ^+ - and σ^- -polarized signals propagate at different velocities and experience different absorption losses. (c) The energy diagram of typical atoms or atomic-like emitters, with degenerate ground Zeeman levels ($|g\rangle$) and the allowing optical transitions to excited energy levels ($|e\rangle$, $|f\rangle$). The drive field ($|g\rangle \rightarrow |e\rangle$) induces the magnetization of the atoms as the population concentrates to one side of the Zeeman levels, which leads to the different response to σ^+ - and σ^- -polarized signals ($|g\rangle \rightarrow |f\rangle$) due to selection rules. (d) The illustration of absorption and dispersion in a magnetized atomic medium for σ^+ - and σ^- -polarized signals. Absorption dominates in the shadow region where the signal is near-resonant to the atomic transitions, while dispersion dominates for off-resonant cases.

quantum photonic chips and explore intriguing topological properties of light [30].

II. RESULTS

A. Principle of OIM-based non-reciprocity

Figures 1(a) and (b) schematically illustrate the general principle of the noiseless all-optical non-reciprocity that is based on the OIM. In the presence of an external circularly-polarized drive field, the optical response of an atom ensemble to a weak signal field is modified, leading to a circular-polarization dependent propagation velocity and absorption. As indicated in Fig. 1(c), the atoms possess hyperfine ground spin states $|g, m_F\rangle$, with m_F denoting the quantum spin number with $|m_F| \leq F_g$. By introducing the ancillary energy level $|e\rangle$ with $E_e \geq E_g$, the drive laser with the σ^+ polarization changes the population of the atoms to $m_F = F_g$, and thus builds up an effective magnetization of the atom spin states (green lines in Fig. 1(c)). For an input signal near-resonant to $|g\rangle \rightarrow |f\rangle$ by $F_f \leq F_g$, the drive laser could transfer the population to $m_F = F_g$, for which the its σ^+ -transition is forbidden (blue

dash line in Fig. 1(c)). Therefore, the atomic medium in Fig. 1(a) is transparent to the σ^+ -polarized signal. In contrast, the transition for the σ^- -polarized signal is allowed (red solid line in Fig. 1(c)), thus the signal propagation is described in the atomic media configuration shown in Fig. 1(b).

Figure 1(d) illustrates the OIM-induced circular birefringence and dichroism, as the polarized medium induces velocity and absorption change to the probe signals. When the circularly polarized probe signal is off-resonant to the atoms (with detuning Δ), the atoms induce effective phase change $\propto 1/\Delta$ while the absorption is suppressed to $\propto 1/\Delta^2$. Different from the conventional Faraday effect, where the external magnetic field induces the Zeeman energy level shifts and thereby circular birefringence, our scheme bases on ground state magnetization of the atoms induced by circularly polarized drive. The scheme is also distinct from previous nonlinear optical schemes [11–21], where the phase-matching condition breaks the time-reversal symmetry of light. The drive field could be applied to any ancillary transition that couples to the target ground levels and is not necessary to be coherent with the signal. Therefore, the scheme allows broad bandwidth non-reciprocity beyond the limitation of phase-matching, permits more convenient filtration of drive laser, and the device would not induce noises for signals. It is also noted that the population condition illustrated in Fig. 1(c) is not strictly required for realizing non-reciprocity, because the time-reversal symmetry could be achieved as long as the uniform population distribution over all m_F states is broken to produce nonzero net spin polarization.

We experimentally implement the proposed scheme based on ^{87}Rb warm atom vapor, as shown in Fig. 2(a). The energy diagram of the atom is shown in the inset, with $|g\rangle = |5^2S_{1/2}, F=2\rangle$ and $|f\rangle = |5^2P_{1/2}, F'=1, 2\rangle$ for the D_1 transitions at $\sim 795\text{nm}$, and we choose the ancillary energy levels $|e\rangle = |5^2P_{3/2}, F'=1, 2, 3\rangle$ corresponding to D_2 transitions at $\sim 780\text{nm}$. First of all, the non-reciprocity via OIM is verified by a circularly polarized drive field ($\sim 780\text{nm}$) on the atoms, with σ^+ -polarized forward (port 1 \rightarrow 2) or σ^- -polarized backward (port 2 \rightarrow 1) signal probing the vapor cell at $\sim 795\text{nm}$. Here, the predicted circular dichroism of atomic medium is converted to non-reciprocal transmittance ($T_{1\rightarrow 2} \neq T_{2\rightarrow 1}$) of linear polarization introduced by way of a pair of quarter waveplates (QWP)(Fig. 2(a)). As plotted in Fig. 2(b), we observe a 20dB isolation with bandwidth of about 740MHz due to the Doppler broadening from the atom transition linewidth of $\sim 6\text{MHz}$. The highest isolation ratio of $30.3^{+0.3}_{-0.2}\text{dB}$ is achieved without a cavity in a single pass configuration (details in Supplementary Information). To valid the mechanism for other atomic media, we also demonstrate the cavity-less isolation by the isotope ^{85}Rb in a vapor cell of natural abundance Rubidium, demonstrating a 900MHz bandwidth and a highest isolation ratio of $29.6^{+0.6}_{-0.6}\text{dB}$. Since the magnetization of the medium could be perturbed by the stray magnetic field perpendicular to the direction of light propagation (B_\perp), the OIM-induced non-reciprocity might be sensitive to magnetic field. However, in our experiments, we found

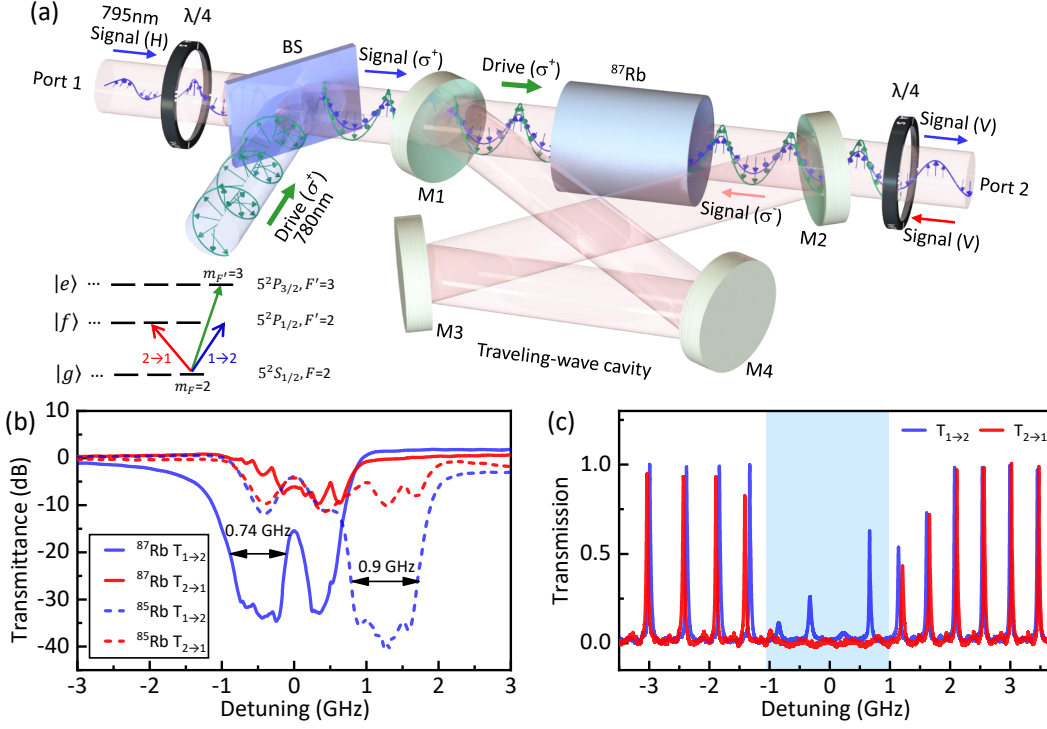


FIG. 2. **Experimental observation of the magnetic-free non-reciprocity in an atom ensemble.** (a) Experimental setup with a traveling-wave cavity, comprising of four mirrors with a Rb vapor cell inside. The linearly polarized input signal from port 1(2) is converted to σ^+ (σ^-) polarization by quarter waveplates (QWP). A drive laser in σ^+ polarization is coupled into the cavity through a beam splitter of port 1. Therefore, the circular birefringence or dichroism leads to non-reciprocal transmission of the whole device system. The inset diagram shows the energy levels of Rb atom, with the arrows representing the drive laser (green), the forward signal laser from port 1 (blue) and the backward signal laser from port 2 (red). (b) The broadband isolation by hot atom ensemble due to optically-induced magnetization, based on the setup in (a) without the cavity. A maximum isolation ratio of $30.3^{+0.3}_{-0.2}$ dB and $29.6^{+0.6}_{-0.6}$ dB is observed for ^{87}Rb and ^{85}Rb , respectively, and the corresponding 20dB-isolation bandwidth are 740MHz and 900MHz. Here, the drive power (P_d) is about 130mW while the signal power (P_s) is about $1\mu\text{W}$. (c) Typical transmission spectra for the cavity setup, with $P_d = 45\text{ mW}$ and $P_s = 1\mu\text{W}$. The blue shadow indicates the absorptive region that exhibits circular dichroism, and the region outside the shadow shows mode splitting due to circular birefringence.

that the isolation is very robust and could be maintained even with $B_{\perp} = 10\text{ Gauss}$. Therefore, the OIM provides a very robust photonic non-reciprocity against experimental imperfections, and also relaxes the requirements of drive laser and operating environment for practical applications.

B. Absorptive and dispersive non-reciprocity.

Since the OIM-induced non-reciprocity strongly depends on the optical depth of the atom medium, which might be a limiting factor for cold atoms or emitters in solids, we investigate the cavity-enhanced non-reciprocity in the following experiments (Fig. 2(a)). Typical spectra of the cavity-enhanced non-reciprocity are shown in Fig. 2(c), where the shadow section corresponds to the absorptive region in Fig. 1(d). Here, the transmission of $T_{2\rightarrow 1}$ is greatly suppressed, while peaks with regular free-spectral range are observed in $T_{1\rightarrow 2}$ transmission. Since the atoms in the vapor cell fly between the reservoir and cavity mode fields, which induces the relaxation of the

OIM, the peaks in the absorptive region show reduced transmittance due to the residual populations on the ground states $m_F < 2$ ($F_g = 2$). In contrast, in the detuned frequency regions, the system shows resonance shift between forward and backward spectra. These observations confirm the absorptive and dispersive non-reciprocity realized by the OIM in the atomic medium (Fig. 1(d)).

In an optical traveling-wave cavity, optical modes of orthogonal polarizations are degenerated. As demonstrated above, the OIM could induce the circular birefringence and circular dichroism and thus lifts the degeneracy between σ^+ - and σ^- -polarized modes in our system. Then, the non-reciprocity is realized by probing the OIM via quarter waveplates, as the signal transmission for port $2 \rightarrow 1$ with σ^- -polarization is rejected by the cavity. For better calibration of the system performance, we probe the σ^- -polarization from the forward direction by utilizing the symmetry of the system, because all optical elements are the same when measuring both σ^+ and σ^- polarization forwardly (T_+ and T_-) except that the angle of waveplate is different. Detailed performances of the optical isolation are summarized in Fig. 3.

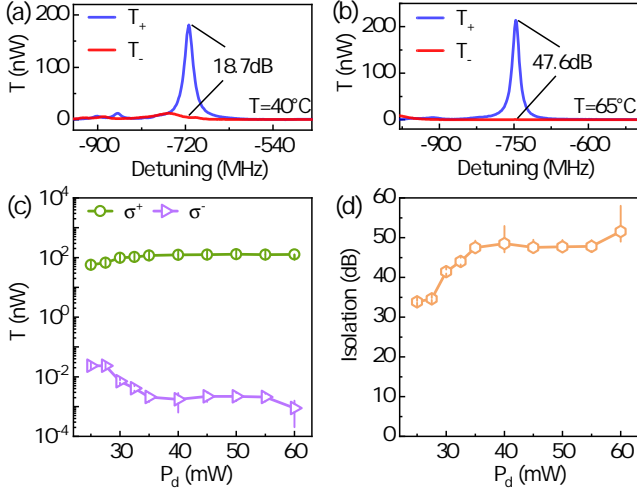


FIG. 3. **Optical isolation via absorptive non-reciprocity.** (a,b) Typical transmission spectra for σ^+ and σ^- -polarized signals at different atomic densities, with the temperature of the atomic cell respectively set at 40°C and 65°C and the corresponding isolation ratios 18.7 dB and 47.6 dB, respectively. Here, the signal and drive power is fixed at $P_s = 50 \mu\text{W}$ and $P_d = 45 \text{ mW}$, respectively. (c) The on-resonant transmitted signal power vs the drive laser power (P_d). The green and purple spots represent the σ^+ and σ^- -polarized signals, respectively. (d) Extracted isolation ratio at different P_d . The largest isolation ratio $51.5^{+6.5}_{-2.5}$ dB is achieved at $P_d = 60 \text{ mW}$. The results in (c) and (d) are measured at 65°C with a fixed signal laser power of $P_s = 50 \mu\text{W}$, and error bars denote standard deviations.

By increasing the temperature of the cell (Fig. 3(a) and (b)), the isolation ratio increases due to the increase of atom density under a fixed drive power P_d of 45 mW. The optical performance also depends on the drive power. As shown in Fig. 3(c), the T_+ is suppressed at low P_d , because the OIM is weak and the atom ensemble is absorptive for both polarizations. By increasing P_d , the atoms are effectively magnetized and become transparent to the σ^+ -polarized signal. Figure 3(d) shows the extracted isolation ratio, which increases with P_d and reaches a maximum of $51.5^{+6.5}_{-2.5}$ dB when $P_d = 60 \text{ mW}$. The linewidth here at 65°C is around $26.5^{+0.2}_{-0.2}$ MHz, primarily determined by the glass-cell-induced loss.

Figure 4 presents the results of the dispersive non-reciprocal effects. The resonance shift $\delta = f_+ - f_-$ of the T_+ and T_- spectra at different temperature are shown in Fig. 4(a), where $f_{+(-)}$ is the resonant frequency of T_+ (T_-) spectrum. Figure 4(b) further details the transmission spectra corresponding to four detuning frequencies indicated in Fig. 4(a). At 65°C and $P_d = 45 \text{ mW}$, we find that the ratio between mode splitting and linewidth δ/γ reaches 4.55, where γ denotes the linewidth of the cavity at f_+ . The δ/γ is a figure-of-merit characterizing OIM for isolator and gyator to account for non-reciprocal phase shift induced by OIM. Furthermore, we find that the relative frequency shift monotonously increases with the vapor temperature as shown in Fig. 4(d) due to the increase of atom density at elevated temperatures.

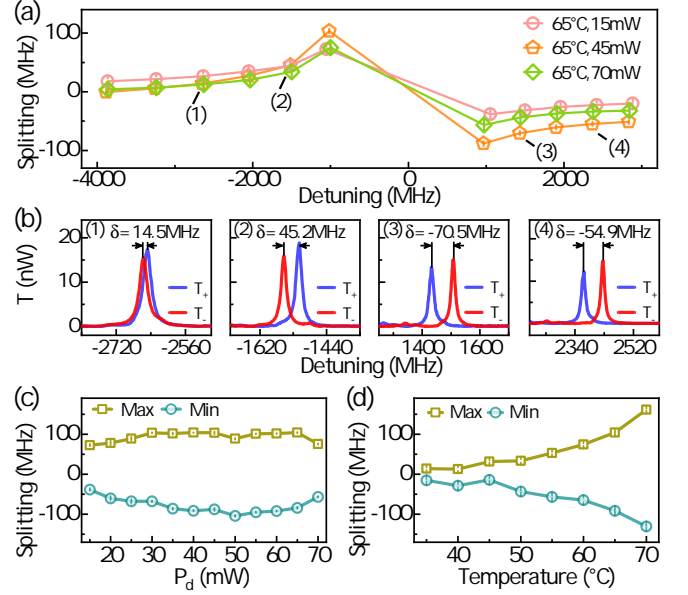


FIG. 4. **Mode frequency shift due to dispersive non-reciprocity.** (a) The resonant frequency shift of two circularly polarized modes at different drive laser power levels (P_d) and fixed cell temperature of 65°C. When the frequency of signal is near-resonant to the atoms (blue shadow region in Fig. 2c), the absorptive effect dominates and the resonances for T_- are suppressed. The dispersive shift can not be distinguished in this regime. (b) The relative mode spectral shifts at four different cavity detunings labeled in (a). (c) and (d) The extracted maximum and minimum mode frequency shifts against P_d and different cell temperatures. In all studies, the signal laser power is fixed at $P_s = 20 \mu\text{W}$, and error bars denote standard deviations.

For the power dependence shown in Fig. 4(c), the frequency shift initially increases and then drops when P_d approaches 70 mW due to population transfer from atomic ground states to the ancillary energy levels ($|f, m_{F'} = 3\rangle$) at high drive intensities, since the drive is coupling with a cyclic transition ($|g, m_F = 2\rangle \rightarrow |f, m_{F'} = 3\rangle$).

C. Noiseless isolation

We lastly demonstrate the inherent noiseless property of our all-optical non-reciprocity via OIM. In the previous demonstration of all-optical non-reciprocity, the strong drive would induce considerable noise by four-wave mixing amplification [18, 19, 21] or the thermal noise occupation of low-frequency excitations [11, 22]. In contrast, there are no such noise processes in our approach that could excite the D_1 transitions by the drive at room temperature, thus there should be no noise photon generated at signal wavelengths. We verify this characteristic over a wide signal power range varying from nano- to milli-Watt, corresponding to an intracavity photon number in the range of $0.84 - 10^6$. As shown in Fig. 5(a), the isolator shows an average of about 37.4 dB isolation with a signal power dynamic range of about 70 dB. Fluctuations

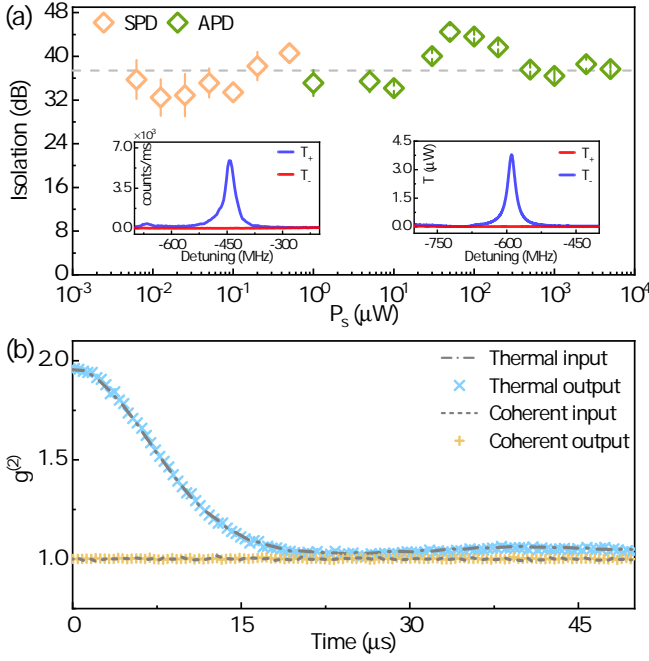


FIG. 5. **The dynamic range and noiseless property of the all-optical isolation.** (a) The measured isolation ratios against input signal power (P_s). Due to the limitation of the system insertion loss and detector's response, avalanche photodetectors (APDs) are adapted for $P_s \geq 1 \mu\text{W}$ (shown as green spots) and a single-photon detector (SPD) is used for $P_s < 1 \mu\text{W}$ (shown as orange spots). The insets are two typical spectra measured for $P_s = 6.25 \text{ nW}$ (left) and 1.2 mW (right), respectively. (b) Measured second-order correlation function ($g^{(2)}$) for signal input to and output from the device. Blue crosses and dashed line are the results for pseudo-thermal source, while yellow crosses and dotted line are the results for coherent source. In all studies, the drive power is set at 50 mW , vapor temperature is 65°C , and error bars denote standard deviations.

of the performance are attributed to the varied response of the detectors at different input power, such as the saturated gain of avalanche photodetector (APD) and counts saturation of single-photon detector (SPD). To quantify the quantum noise properties of OIM, we measure the second-order correlation function ($g^{(2)}(t)$) with a delay time t of transmitted signals, since a noiseless photonic device should conserve the quantum statistics of the input signal. As presented in Fig. 5(b), the $g^{(2)}(t)$ is measured for both coherent laser and pseudo-thermal light source (see Method and Supplementary Information for details). By comparing the $g^{(2)}(t)$ curves for input and output signal, we find the isolator conserves the quantum statistics of these signals. Assuming possible stray thermal and coherent photons detected by SPD, we estimate the equivalent added intracavity noise photon number is $n_{\text{add}} \sim 0.0084$ (See Supplementary Materials for details), which confirms the noiseless non-reciprocity mechanism proposed in this work.

III. DISCUSSION

Comparing to previously demonstrated all-optical non-reciprocity originated from coherent nonlinear processes, the optically-induced atomic magnetization is an incoherent process, thus is very robust against experimental imperfections, such as the drive frequency and amplitude fluctuations, inhomogeneous transition frequency broadening, imperfect circular polarization and beam alignment, as well as stray magnetic fields. The demonstrated noiseless non-reciprocity only requires an atomic ensemble with degenerate Zeeman energy levels, thus the mechanism is extendable to many atoms or atom-like emitters, including hot and cold atoms, molecules, as well as emitters in solids (such as NV centers and rare-earth atoms). Thus, the high-performance isolation is achievable even in UV and mid-IR wavelengths, where commercial products have very limited performance. On a photonic chip, the optically-induced magnetization could be conveniently implemented by harnessing the spin-orbit coupling of photon [28, 31, 32]. Furthermore, our approach could be generalized to other particles or quasi-particles other than photons, such as phonons by utilizing their interaction with electron spins in solids [33]. Aside from the potential applications, our work also merits new physics by taking the degenerate ground Zeeman energy levels into cavity quantum electrodynamics (QED) [34] and waveguide QED, where interesting non-reciprocal phenomena arise, such as non-reciprocal multi-stability, quantum frequency conversion, photon storage and lasing.

* These two authors contributed equally to this work.

† zhangpengfei@sxu.edu.cn

‡ chunhua@ustc.edu.cn

§ clzou321@ustc.edu.cn

- [1] R. J. Potton, "Reciprocity in optics," *Rep. Prog. Phys.* **67**, 717 (2004).
- [2] M. Teich and B. Saleh, eds., *Fundamentals of photonics*, 2nd ed. (Wiley-Interscience, 2007).
- [3] V. Asadchy, M. S. Mirmoosa, A. Díaz-Rubio, S. Fan, and S. A. Tretyakov, "Tutorial on Electromagnetic Nonreciprocity and Its Origins," *arXiv Preprint: 2001.04848* (2020).
- [4] D. Jalas, A. Petrov, M. Eich, W. Freude, S. Fan, Z. Yu, R. Baets, M. Popović, A. Melloni, J. D. Joannopoulos, M. Vanwolleghem, C. R. Doerr, and H. Renner, "What is – and what is not – an optical isolator," *Nat. Photonics* **7**, 579 (2013).
- [5] P. J. Stephens, "Magnetic Circular Dichroism," *Annu. Rev. Phys. Chem.* **25**, 201 (1974).
- [6] W. Kaminsky, "Experimental and phenomenological aspects of circular birefringence and related properties in transparent crystals," *Rep. Prog. Phys.* **63**, 1575 (2000).
- [7] H. Dötsch, N. Bahlmann, O. Zhurumskyy, M. Hammer, L. Wilkens, R. Gerhardt, P. Hertel, and A. F. Popkov, "Applications of magneto-optical waveguides in integrated optics: review," *J. Opt. Soc. Am.* **22**, 240 (2005).
- [8] L. Bi, J. Hu, P. Jiang, D. H. Kim, G. F. Dionne, L. C. Kimerling, and C. a. Ross, "On-chip optical isolation in monolithically in-

- tegrated non-reciprocal optical resonators,” *Nat. Photonics* **5**, 758 (2011).
- [9] L. Fan, C.-L. Zou, R. Cheng, X. Guo, X. Han, Z. Gong, S. Wang, and H. X. Tang, “Superconducting cavity electro-optics: A platform for coherent photon conversion between superconducting and photonic circuits,” *Sci. Adv.* **4**, eaar4994 (2018).
- [10] A. W. Elshaari, W. Pernice, K. Srinivasan, O. Benson, and V. Zwiller, “Hybrid integrated quantum photonic circuits,” *Nat. Photonics* **14**, 285 (2020).
- [11] Z. Shen, Y.-L. Zhang, Y. Chen, C.-L. Zou, Y.-F. Xiao, X.-B. Zou, F.-W. Sun, G.-C. Guo, and C.-H. Dong, “Experimental realization of optomechanically induced non-reciprocity,” *Nat. Photonics* **10**, 657 (2016).
- [12] F. Ruesink, M.-A. Miri, A. Alù, and E. Verhagen, “Non-reciprocity and magnetic-free isolation based on optomechanical interactions,” *Nat. Commun.* **7**, 13662 (2016).
- [13] Z. Shen, Z. Yanlei, Y. Chen, F.-W. Sun, X.-B. Zou, G.-C. Guo, C.-L. Zou, and C. Dong, “Reconfigurable optomechanical circulator and directional amplifier,” *Nat. Commun.* **9**, 1797 (2017).
- [14] E. Verhagen and A. Alù, “Optomechanical nonreciprocity,” *Nat. Phys.* **13**, 922 (2017).
- [15] C.-H. Dong, Z. Shen, C.-L. Zou, Y.-L. Zhang, W. Fu, and G.-C. Guo, “Brillouin-scattering-induced transparency and non-reciprocal light storage,” *Nat. Commun.* **6**, 6193 (2015).
- [16] J. Kim, M. C. Kuzyk, K. Han, H. Wang, and G. Bahl, “Non-reciprocal Brillouin scattering induced transparency,” *Nat. Phys.* **11**, 275 (2015).
- [17] S. Zhang, Y. Hu, G. Lin, Y. Niu, K. Xia, J. Gong, and S. Gong, “Thermal-motion-induced non-reciprocal quantum optical system,” *Nat. Photonics* **12**, 744 (2018).
- [18] S. Hua, J. Wen, X. Jiang, Q. Hua, L. Jiang, and M. Xiao, “Demonstration of a chip-based optical isolator with parametric amplification,” *Nat. Commun.* **7**, 13657 (2016).
- [19] E.-Z. Li, D.-S. Ding, Y.-C. Yu, M.-X. Dong, L. Zeng, W.-H. Zhang, Y.-H. Ye, H.-Z. Wu, Z.-H. Zhu, W. Gao, G.-C. Guo, and B.-S. Shi, “Experimental demonstration of cavity-free optical isolators and optical circulators,” *arXiv preprint: 1908.07210* (2019).
- [20] K. Xia, F. Nori, and M. Xiao, “Cavity-free optical isolators and circulators using a chiral cross-Kerr nonlinearity,” *Phys. Rev. Lett.* **121**, 203602 (2018).
- [21] G. Lin, S. Zhang, Y. Hu, Y. Niu, J. Gong, and S. Gong, “Non-reciprocal amplification with four-level hot atoms,” *Phys. Rev. Lett.* **123**, 033902 (2019).
- [22] K. Fang, J. Luo, A. Metelmann, M. H. Matheny, F. Marquardt, A. A. Clerk, and O. Painter, “Generalized non-reciprocity in an optomechanical circuit via synthetic magnetism and reservoir engineering,” *Nat. Phys.* **13**, 465 (2017).
- [23] M. Aidelsburger, S. Nascimbene, and N. Goldman, “Artificial gauge fields in materials and engineered systems,” *C. R. Phys.* **19**, 394 (2018).
- [24] Z. Yu and S. Fan, “Complete optical isolation created by indirect interband photonic transitions,” *Nat. Photonics* **3**, 91 (2009).
- [25] K. Fang, Z. Yu, and S. Fan, “Realizing effective magnetic field for photons by controlling the phase of dynamic modulation,” *Nat. Photonics* **6**, 782 (2012).
- [26] D. L. Sounas and A. Alù, “Non-reciprocal photonics based on time modulation,” *Nat. Photonics* **11**, 774 (2017).
- [27] D. B. Sohn, S. Kim, and G. Bahl, “Time-reversal symmetry breaking with acoustic pumping of nanophotonic circuits,” *Nat. Photonics* **12**, 91 (2018).
- [28] C. Sayrin, C. Junge, R. Mitsch, B. Albrecht, D. O’Shea, P. Schneeweiss, J. Volz, and A. Rauschenbeutel, “Nanophotonic optical isolator controlled by the internal state of cold atoms,” *Phys. Rev. X* **5**, 041036 (2015).
- [29] M. Scheucher, A. Hilico, E. Will, J. Volz, and A. Rauschenbeutel, “Quantum optical circulator controlled by a single chirally coupled atom,” *Science* **354**, 1577 (2016).
- [30] T. Ozawa, H. M. Price, A. Amo, N. Goldman, M. Hafezi, L. Lu, M. C. Rechtsman, D. Schuster, J. Simon, O. Zilberberg, and I. Carusotto, “Topological photonics,” *Rev. Mod. Phys.* **91**, 015006 (2019).
- [31] I. Söllner, S. Mahmoodian, S. Lindskov Hansen, L. Midolo, A. Javadi, G. Kirsanske, T. Pregnolato, H. El-Ella, E. Hye Lee, J. Dong Song, S. Stobbe, and P. Lodahl, “Deterministic photon-emitter coupling in chiral photonic circuits,” *Nat. Nanotechnol.* **10**, 775 (2015).
- [32] P. Lodahl, S. Mahmoodian, S. Stobbe, P. Schneeweiss, J. Volz, A. Rauschenbeutel, H. Pichler, and P. Zoller, “Chiral quantum optics,” *Nature* **541**, 473 (2017).
- [33] D. A. Golter, T. Oo, M. Amezcua, K. A. Stewart, and H. Wang, “Optomechanical Quantum Control of a Nitrogen-Vacancy Center in Diamond,” *Phys. Rev. Lett.* **116**, 143602 (2016).
- [34] P. Yang, M. Li, X. Han, H. He, G. Li, C.-L. Zou, P. Zhang, and T. Zhang, “Non-reciprocal cavity polariton,” *arXiv Preprint: 1911.10300* (2019).

Acknowledgments

We would like to thank Shu-Hao Wu and Ji-Zhe Zhang for the assistance in collecting and processing data, Ming Li and Xin-Biao Xu for helpful discussions. The work was supported by the National Key R&D Program of China (Grant No. 2016YFA0301303), the National Natural Science Foundation of China (Grant No. 11922411, 11874342, 11704370, 11874342, and 91536219), and Anhui Initiative in Quantum Information Technologies (Grant No. AHY130200). P. Z, G. L. and T. Z. were supported by National Key R&D Program of China (Grant No. 2017YFA0304502), the National Natural Science Foundation of China (Grants No. 11974225, No. 11574187, No. 11674203, No. 11974223, and No. 11634008), and the Fund for Shanxi “1331 Project” Key Subjects Construction. C.-L.Z. was also supported by the Program of State Key Laboratory of Quantum Optics and Quantum Optics Devices (No. KF201809).

Author contributions

C.-L.Z., X.-X.H., G.L. and H.T. conceived the experiments. X.-X.H., Z.-B.W. and P.Z. built the experimental setup and carried out the measurements with the assistance by G.-J.C., G.L. and T.Z. X.-X.H., Z.-B.W. and C.-L.Z. analyzed the data, Y.-L.Z. and X.-B.Z. provided theoretical supports. C.-L.Z., X.-X.H. and P.Z. wrote the manuscript with input from all co-authors. C.-H.D., G.-C.G. and C.-L.Z. supervised the project. All authors contributed extensively to the work presented in this paper.